forests

MDPI

Article

Disentangling Mechanisms of Drought-Induced Dieback in *Pinus nigra* Arn. from Growth and Wood Isotope Patterns

Ester González de Andrés and Jesús Julio Camarero *

Pyrenean Institute of Ecology (IPE-CSIC), 50192 Zaragoza, Spain; ester.gonzalez@ipe.csic.es
* Correspondence: jjcamarero@ipe.csic.es; Tel.: +34-976-363-222 (ext. 880041)

Received: 19 November 2020; Accepted: 14 December 2020; Published: 16 December 2020

Abstract: The increased frequency and intensity of warming-induced droughts have triggered dieback episodes affecting many forest types and tree species worldwide. Tree plantations are not exempt as they can be more vulnerable to drought than natural forests because of their lower structural and genetic diversity. Therefore, disentangling the physiological mechanisms leading to growth decline and tree mortality can provide tools to adapt forest management to climate change. In this study, we investigated a *Pinus nigra* Arn. plantation situated in northern Spain, in which some trees showed canopy dieback and radial-growth decline. We analyzed how radial growth and its responses to drought events differed between non-declining (ND) and declining (D) trees showing low and high canopy defoliation, respectively, in combination with carbon ($\delta^{13}C$) and oxygen ($\delta^{18}O$) isotope ratios in tree rings. The radial growth of *P. nigra* was constrained by water availability during the growing season and the previous autumn. The radial growth of D trees showed higher sensitivity to drought than ND trees. This fact is in accordance with the lower drought resilience and negative growth trends observed in D trees. Both tree classes differed in their growth from 2012 onwards, with D trees showing a reduced growth compared to ND trees. The positive $\delta^{13}C$-$\delta^{18}O$ relationship together with the uncoupling between growth and intrinsic water-use efficiency suggest that D trees have less tight stomatal regulation than ND trees, which could involve a high risk of xylem embolism in the former class. Our results suggest that different water use strategies between coexisting ND and D trees were behind the differences in growth patterns and point to hydraulic failure as a possible mechanism triggering dieback and growth decline.

Keywords: basal area increment; carbon isotopes; drought; growth decline; intrinsic water-use efficiency; oxygen isotopes; resilience; tree plantation

1. Introduction

Increasing rates of tree mortality and dieback events have been reported worldwide, covering all major forested biomes on Earth [1–7]. These trends have been linked to warming and drought, sometimes co-occurring with insect outbreaks [1]. Climatic models forecast an increase in extreme climatic events globally [8,9]; thus, drought-related growth decline and tree mortality are likely to intensify [10]. Widespread episodes of forest dieback and mortality have important consequences for biodiversity, ecosystem function and services, and feedbacks to climate change through biophysical effects and the loss of carbon sinks [11].

The impacts of climate change can be stronger in pine plantations that have been found to be more vulnerable to warming-related drought than naturally regenerated forests [12,13]. Pine plantations constitute ca. 7% of the total worldwide forest cover, and they amount to 10% in the Mediterranean Basin [14]. Over this region, massive pine reforestations were developed during the 20th century to

increase forest productivity, to protect the soil against erosion and to restore watersheds on formerly deforested lands derived from traditional uses [15]. This resulted in very homogeneous forests of pioneer pine species that have been affected by striking episodes of drought-triggered canopy dieback, growth decline and mortality [16–21]. Therefore, a proper understanding of the mechanisms leading to mortality and shaping differences among individual trees can help to improve the management of tree plantations.

Hydraulic failure and carbon starvation have been proposed as the two main mechanisms inducing drought-related tree dieback [22–24]. Hydraulic failure refers to the cessation of symplastic biochemical functioning and the disruption of water transport through xylem embolism [25], whereas carbon starvation consists of a strong reduction in carbon pools that prevent the maintenance of cellular and defensive metabolisms [22]. Moreover, such mechanisms interact with biotic agents [26] and nutritional aspects [27]. The predisposition of trees to drought-induced mortality can be assessed using a dendrochronological retrospective approach. Tree ring width data offer an easily available long-term record of radial growth variability [28]. Indeed, dendrochronological studies comparing conspecific trees with different vitality (e.g., defoliation percentage) growing in the same stand have provided interesting insights into the short- and long-term growth patterns before tree death [2,6,29]. For instance, Camarero et al. [6] showed that legacy effects resulting from severe droughts can last for several years and they are usually greater in later dying trees. However, growth patterns per se may not be enough to disentangle the physiological mechanisms leading to tree mortality.

Stable isotope ratios in tree rings can help to overcome this issue because they contain retrospective information on the ecophysiological processes experienced by trees [30]. The processes of assimilation of carbon and oxygen are strongly influenced by climate. Therefore, the so-called dual-isotope composition approach is a useful tool to elucidate shifts in the relationship between photosynthetic rate (A) and stomatal conductance (g_S) rates, that is, intrinsic water-use efficiency (iWUE). On one hand, gas exchange modifications are captured in the composition of stable carbon isotopes ($\delta^{13}C$) of tree rings owing to the connection between carbon isotope fractionation during photosynthesis and the ratio of CO_2 concentration between the intercellular space and the atmosphere [31]. Conversely, the $\delta^{18}O$ is related to g_S through the influence of vapor pressure deficit [32] and transpirational dilution of evaporatively enriched leaf water [33]. Therefore, it can help to unravel the effects of drought on A and g_S, after considering the variations in tree ring $\delta^{18}O$ signature resulting from differences in $\delta^{18}O$ water sources associated with changes in soil water uptake depth [34].

In this study, we aimed at analyzing the mechanisms underlying the growth decline and canopy dieback of some trees in a *Pinus nigra* Arn. plantation situated in north Spain. This species is widely distributed in mid-altitude Mediterranean forests and in temperate woodlands in central-eastern Europe, where it has been used extensively in reforestation and land rehabilitation due to its ecological flexibility [35]. For that purpose, we combined a retrospective reconstruction of long-term radial growth patterns and growth responses to severe drought events with carbon and oxygen isotope ratios. We hypothesized that successive drought events during the last decades affected symptomatic and asymptomatic trees differently, showing high and low defoliation levels, respectively, due to the less conservative use of water of symptomatic trees increasing their risk of hydraulic failure [30,36].

2. Materials and Methods

2.1. Study Site and Climate Data

The Sabaiza forest (42°37′57′′ N, 1°26′06′′ W, 865–900 m a.s.l.) is located in the Ezprogui municipality, Navarra province (northern Spain) (Figure 1a). The study stand is a *Pinus nigra* subsp. *Nigra* (Hoss) var. *austriaca* plantation carried out during the 1950s and 1960s with the objective of increasing forest productivity and minimizing soil loss as well as soil erosive processes. The soil type is xerochrepts, the aspect is E-SE and the slope 23°. The stand accounts for a density of 720 trees ha^{-1}, a basal area of 24.9 m^2 ha^{-1}, an average diameter at 1.3 m (DBH) of 23.9 ± 1.2 cm and an average tree

height of 11.5 ± 0.3 m. The main understory species are *Buxus sempervirens* L., *Juniperus communis* L., and *Rubus ulmifolius* Schott. No thinning has been carried out in the study stands for the past thirty years, but they have started showing dieback symptoms (leaf loss and shoot dieback, elevated mortality rate) since the mid-2010s. Some trees exhibit severe defoliation (>80%) due to outbreaks of the pine processionary moth (*Thaumetopoea pityocampa* Denis and Schiffermüller). Caterpillar nests were first observed in winter 2016–2017 and again in winter 2017–2018. Herbivory on old needles finishes in late winter, when caterpillars leave trees and bury in the soil.

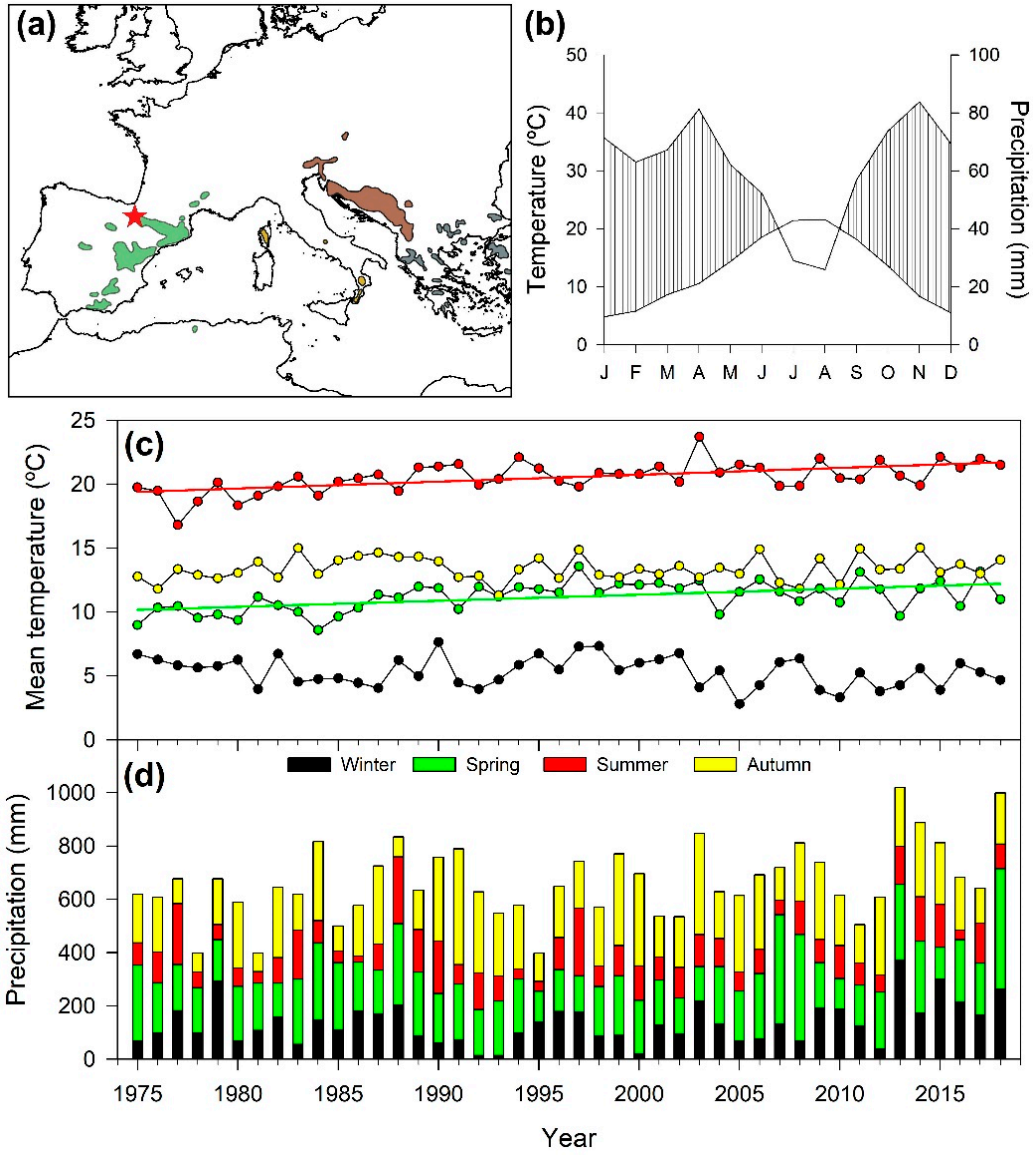

Figure 1. (**a**) Location of the study plantation (red star) in northern Spain. Natural distribution of *Pinus nigra* subspecies are highlighted in different colors: *salzmannii* (green), *nigra* (brown), *laricio* (yellow) and *pallasiana* (grey) [37]. (**b**) Climate diagram of Lerga climate station located near the study site. Mean temperature (**c**) and precipitation (**d**) seasonal trends for the 1975–2018 period. Seasons are as follows: winter (DJF), spring (MAM), summer (JJA) and autumn (SON). Lines correspond to significant trends ($p < 0.05$). Lines represent significant trends in seasonal climatic series.

The climate in the study area is cold-wet Mediterranean, characterized by dry and warm summers and wet and mild springs and autumns. We retrieved the monthly maximum and minimum temperature and precipitation data from the nearest weather station (Lerga station, 42°33′54′′ N, 1°30′04 W,

612 m a.s.l.) for the period 1975–2018. The mean annual temperature is 12.6 °C. July and August are the months with higher temperatures (average maximum temperature of 28.1 °C), while January is the coldest month (average minimum temperature of 1.4 °C). The mean annual precipitation is 736 mm, where the driest and wettest months are August (26 mm) and November (84 mm), respectively (Figure 1b).

We estimated the monthly potential evapotranspiration (PET) using the modified form of the Hargreaves equation [38]. Then, we calculated the Standardized Precipitation Evaporation Index (SPEI), which is a multi-scalar drought index based on the accumulated water deficit (water balance), as the difference between monthly precipitation and monthly PET [39]. We calculated the SPEI at different timescales from 1 to 18 months.

2.2. Field Sampling and Dendrochronological Procedures

We sampled 10 couples of dominant non-declining (ND) and declining (D) trees ($n = 20$) in autumn 2018. We assessed defoliation by a visual assessment of crown transparency in 2018, and it was considered a proxy of tree vigor following previous studies on drought-stressed pines [6]. We selected the trees based on their defoliation levels by considering neighboring individuals showing high (>60%, D trees) and low (<40%, ND trees) canopy defoliation, respectively. This threshold was selected based on similar research which showed that a defoliation threshold of 60% allowed discriminating trees with different vigor [13]. Both ND and D trees produced shoots and needles in 2018, despite the fact that D trees were always more defoliated. We avoided sampling D trees affected by defoliation caused by the pine processionary moth, i.e., presenting caterpillar nests or needles eaten by this herbivore.

We took wood cross-sections at 1.3 m. The samples were air-dried and sanded until tree rings were clearly visible [28]. We visually cross-dated all samples and the tree ring width was measured to a precision of 0.01 mm along two opposite radii per sample (separated by 180°) using a LINTAB measuring device (Frank Rinn, Heidelberg, Germany). We further validated cross-dating using the COFECHA software, which calculates moving correlations among individual tree series [40]. We transformed tree ring width series to basal area increment (BAI) series using the following equation and assuming concentric rings:

$$\mathrm{BAI} = \pi \left({R^2}_t - {R^2}_{t-1} \right) \quad (1)$$

where ${R^2}_t$ and ${R^2}_{t-1}$ are the radii corresponding to the years t and $t-1$, respectively. We used BAI because it is a two-dimensional measure of stem increment in area that is known to better reflect the growth of the whole tree than one-dimensional tree ring width [41].

We developed mean residual BAI chronologies for each tree vigor class to calculate climate-growth associations. Firstly, we removed non-climatic biological growth trends of individual tree ring width series by fitting a horizontal line using the mean of the series. Afterwards, an autoregressive model was applied to each detrended series to remove most of the first-order autocorrelation. Finally, we obtained mean chronologies of ND and D trees using a bi-weight robust mean.

2.3. Growth Responses to Drought

We identified drought events based on the SPEI series calculated for the month and timescale that best correlated with BAI chronologies. The years with 10% lower SPEI values were selected considering the reference period 1975–2018. If two events were separated by less than three years, the lowest value was chosen. We evaluated the short-term growth responses to drought by means of the three resilience indices proposed by Lloret et al. [42]. Resistance (*Rt*), calculated with the ratio $\mathrm{BAI_D/BAI_{preD}}$, characterizes the ability of the tree to revoke the stress situation induced by the drought event. Recovery (*Rc*) reflects the extent of growth increase or decrease after the drought event. *Rc* is estimated as $\mathrm{BAI_{postD}/BAI_D}$. Resilience (*Rs*) indicates the ability of a tree to reach a pre-drought growth level and it is calculated as $\mathrm{BAI_{postD}/BAI_{preD}}$. $\mathrm{BAI_D}$ is the BAI during the corresponding drought year, and $\mathrm{BAI_{preD}}$ and $\mathrm{BAI_{postD}}$ are the average BAI for the 3 years preceding and following the drought

event, respectively. We chose consistent preD and postD periods of 3 years based on previous studies as this represents a good compromise between drought intensity and the short-term growth response [43]. We also quantified the long-term growth responses after selected drought events. For that purpose, we estimated trends in mean BAI series since the drought event to 2018.

2.4. Stable Isotope Analyses and Water-Use Efficiency

We performed the carbon and oxygen isotope analyses on five trees of each vigor class for the period 1975–2018. We selected the trees based on their highest BAI correlations with the mean BAI series of each vigor class. We separated the tree rings manually using a scalpel and pooled them at tree-level in groups of five contiguous rings (e.g., 1975–1979, 1980–1984, etc.; n = 9 samples per tree). We milled each group of five tree rings using a ball mill (Retsch ZM1, Haan, Germany). Then, we extracted α-cellulose with a double-step digestion [44].

The stable isotope composition was measured at the Stable Isotope Facility (University of California, Davis, CA, USA). The carbon isotope composition was analyzed using a PDZ Europa ANCA-GSL elemental analyzer interfaced to a PDZ Europa 20-20 isotope ratio mass spectrometer (Sercon Ltd., Cheshire, UK). The oxygen isotope composition was analyzed using an elementar PyroCube (Elementar Analysensysteme GmbH, Hanau, Germany) interfaced to an Isoprime VisION (Isoprime Ltd., Stockport, UK, a unit of Elementar Analysensysteme GmbH, Hanau, Germany). The results were expressed as isotopic composition of carbon (δ^{13}C) and oxygen (δ^{18}O) relative to Vienna Pee Dee Belemnite and Vienna Standard Mean Ocean Water standards, respectively [45]. The accuracy of the analyses (SD of working standards) was 0.05–0.21‰.

We used δ^{13}C to calculate the iWUE, that is, the ratio between the photosynthetic rate (A) and its stomatal conductance (g_S), using the following equation [31]:

$$\text{iWUE} = Ca \times [1 - (Ci/Ca)] \times 0.625 \quad (2)$$

where Ca and Ci are CO_2 concentrations in the atmosphere and the intercellular space, respectively, and 0.625 is the relation among conductance of H_2O and CO_2. To determine Ci, we used the following equation:

$$Ci = Ca\ [(\delta^{13}\text{Ctree} - \delta^{13}\text{Catm} + 1)/(b - a)] \quad (3)$$

where δ^{13}Ctree and δ^{13}Catm are the tree and atmospheric C isotope compositions, respectively, a is the diffusion fractionation across the boundary layer and the stomata (+4.4‰) and b is the Rubisco enzymatic biologic fractionation (+27.0‰). We used δ^{13}Catm estimated values for the period 1975–2003 from [46], and the measured values for the 2004–2018 period were retrieved from the Earth Research Laboratory website (http://www.esrl.noaa.gov/).

2.5. Statistical Analyses

We used the Kendall τ statistic to assess trends in climatic and growth series. We performed comparisons between ND and D trees regarding size (DBH and height), mean values of radial growth (BAI) and isotope data (δ^{13}C, δ^{18}O and iWUE) through time, as well as compared differences in short-term growth responses to drought, using Wilcoxon rank-sum tests. We analyzed the relationships between climatic variables and radial growth (residual BAI chronologies) for each tree vigor class using Pearson correlations, which were calculated from 1- to 18-month timescales and from January to December. We used linear mixed effects models [47] to test the relationship between stable isotope variables and growth, which was logarithmically transformed to normalize its distribution. Since these measurements represent repeated measures over the same individual trees, tree identity was included as a random factor.

We performed all statistical analyses in R (version 3.6.3, Vienna, Austria) [48]. The *SPEI* package [49] was employed for PET and SPEI calculation. The *dplR* package [50] was used to convert annual ring measurements into BAI and to detrend growth series and develop residual BAI chronologies. Kendall

trends were calculated with the *Kendall* package [51]. The *nlme* package [52] was used to perform linear mixed effects models.

3. Results

3.1. Tree Ring Width Statistics of Species Mean Chronologies

Significant positive trends were found for maximum spring and summer temperatures since 1975 at the study area (Figure 1c), whereas the mean winter minimum temperature has decreased during the last decades. No significant trends were found for precipitation (Figure 1d). There were no significant differences in DBH ($W = 47.5$, $p = 0.561$) or height ($W = 30.0$, $p = 0.377$) between the two tree vigor classes.

The radial growth of both ND and D trees followed similar patterns, with BAI reaching a maximum in the mid-1990s. Afterwards, both vigor classes showed a reduction in their growth rate. This tendency was more pronounced for D trees, and this vigor class displayed a significantly ($p < 0.005$) lower growth than ND trees after 2012 (9.93 ± 1.03 cm^2 of ND trees vs. 5.99 ± 0.87 cm^2 of D trees during the 2012–2018 period) (Figure 2a).

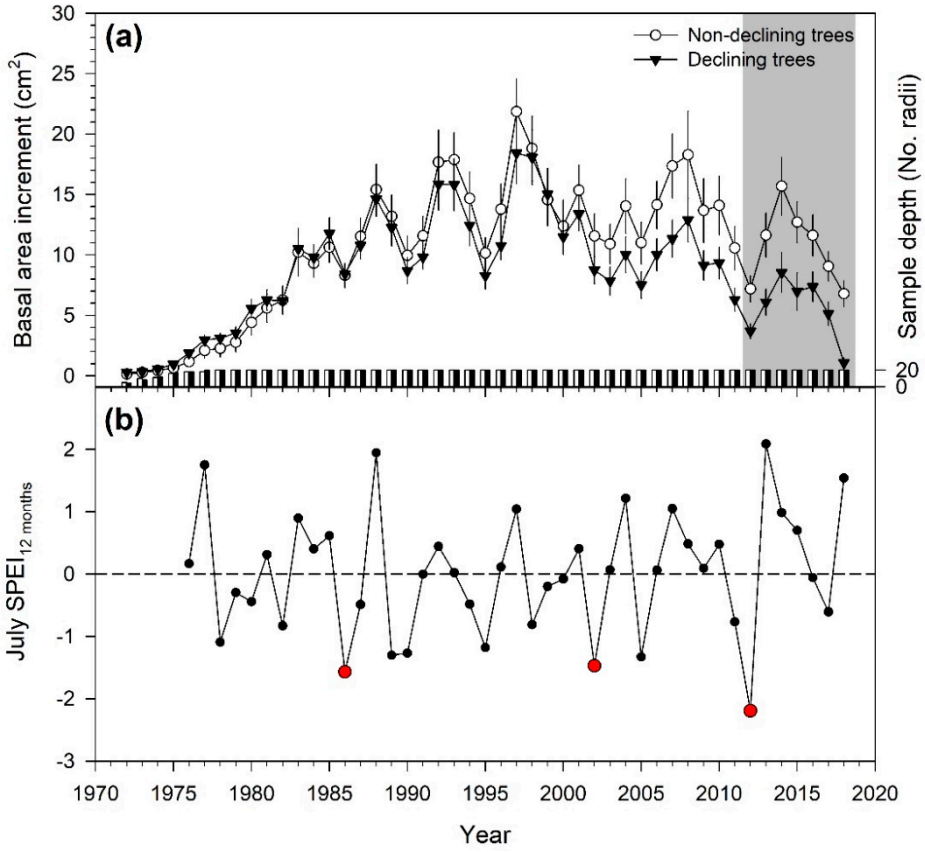

Figure 2. (**a**) Mean basal area increment (BAI) of non-declining (empty circles) and declining (black triangles) trees. The bottom bars represent the number of radii measured every year (sample depth). Error bars correspond to standard errors. The grey filled area indicates the period when BAI of ND and D trees significantly ($p < 0.05$) differed. (**b**) Values of the July Standardized Precipitation Evaporation Index (SPEI) calculated at 12-month scale. The month and SPEI scale were selected based on the highest correlations found between SPEI and residual BAI chronologies. The red symbols indicate drought events (1986, 2002 and 2012).

The highest correlations between the water balance and growth of both ND and D trees were found with the July SPEI calculated at a 12-month timescale, that is, including an accumulated water deficit

of one year (Figure 3). Growth sensitivity to drought was higher in D trees than in ND trees (July SPEI 12-month correlations: ND trees $r = 0.568$, $p < 0.001$; D trees $r = 0.637$, $p < 0.001$). The July 12-month SPEI series were evaluated to identify extreme drought events for the study period (1975–2018). The lowest SPEI values corresponded to 1986, 2002 and 2012 (Figure 2b). Hence, they were identified as the more relevant drought events during the study period. Although the SPEI value of 2005 (SPEI = −1.430) was included within the 10% lower values, it was only three years apart from the 2002 drought (SPEI = −1.497) so it was not considered.

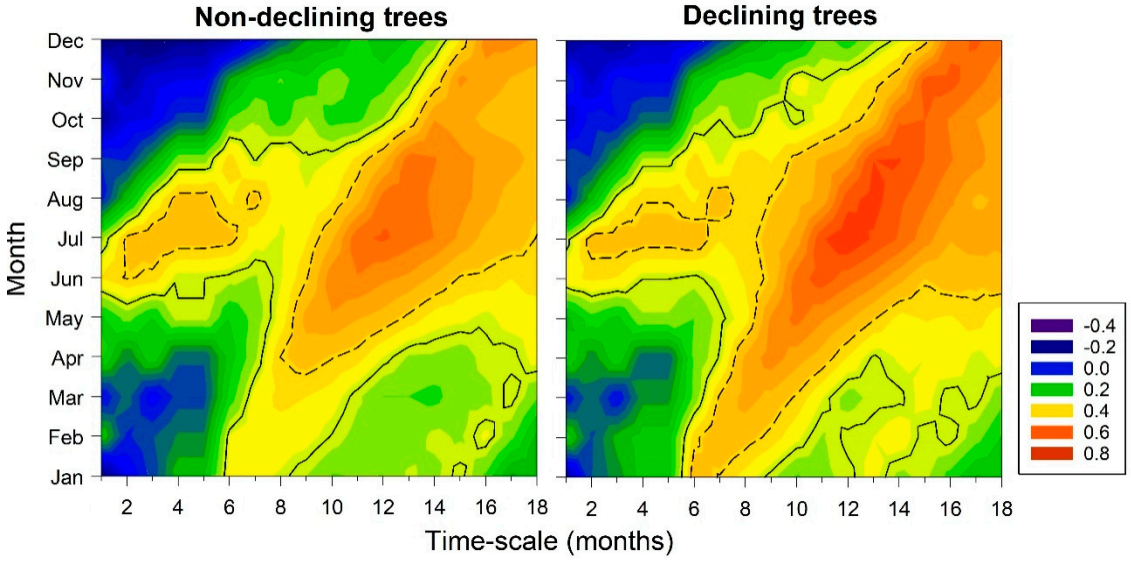

Figure 3. Correlation coefficients (see color scale) calculated between residual BAI chronologies and the SPEI drought index at different timescales for non-declining (**left** panel) and declining trees (**right** panel). Solid and dash lines frame significant correlations at 0.05 and 0.01 levels, respectively.

Short-term growth reductions after drought events were important in the two tree vigor classes (54.9% and 72.3% in ND and D trees, respectively). They resulted in *Rt* values < 1 (Table 1). *Rt* and *Rc* were significantly higher in ND trees than in D trees in 2002 and 2012, respectively. As a consequence, the *Rs* values of D trees were significantly lower than those of ND trees after the last two study droughts: 2002 and 2012. The long-term growth trends after droughts (considering the period since the drought event until 2018) were negative ($p < 0.005$) for D trees, but they were not significant for ND trees.

Table 1. Short- and long-term term growth responses to drought. Short-term (three years long) responses were assessed by resistance (*Rt*), recovery (*Rc*) and resilience (*Rs*) indices values (mean ± standard error) between non-declining (ND) and declining (D) *P. nigra* trees. Different letters indicate significant ($p < 0.005$) statistical differences between tree vigor classes in *Rt*, *Rc* and *Rs* based on Wilcoxon rank-sum tests. Long-term trends are based on the Kendall τ statistic and the slope for linear rate of change was computed from the study drought year until 2018 (i.e., 33, 17 and 7 years long for the 1986, 2002 and 2012 drought events, respectively). Significant ($p < 0.05$) trends are indicated with asterisks (*).

Year	Vigor Class	Short-Term			Long-Term Trend (cm^2 yr^{-1})
		Rt	*Rc*	*Rs*	
1986	ND	0.850 ± 0.049 a	1.634 ± 0.157 a	1.423 ± 0.198 a	−0.086
	D	0.831 ± 0.075 a	1.572 ± 0.132 a	1.276 ± 0.107 a	−0.221 *
2002	ND	0.831 ± 0.041 a	1.076 ± 0.063 a	0.884 ± 0.050 a	−0.194
	D	0.669 ± 0.030 b	0.943 ± 0.078 a	0.633 ± 0.062 b	−0.264 *
2012	ND	0.481 ± 0.041 a	2.419 ± 0.256 a	1.104 ± 0.070 a	−0.146
	D	0.450 ± 0.038 a	1.760 ± 0.176 b	0.814 ± 0.129 b	−0.211 *

3.2. Isotope Signals in Tree Rings

The carbon-related isotopic variables ($\delta^{13}C$ and iWUE) did not show significant differences ($p < 0.05$) between D and ND trees during the period 1975–2000. However, when the growth between ND and D trees significantly differed, that is, when dieback intensified, D trees displayed lower $\delta^{13}C$ values than ND trees (Figure 4). Likewise, D trees showed a lower iWUE during the 2000–2018 period than ND trees, with reductions of 6.6% in iWUE in D trees compared with ND trees since 2000. Considering $\delta^{18}O$, D trees showed lower values than ND trees throughout the last two decades, although significant differences were only found during the 2005–2009 and 2015–2018 periods. BAI was positively associated with iWUE in ND trees (ND trees: $F = 4.072$, $p = 0.047$; D trees: $F = 1.969$, $p = 0.170$) (Figure 5a). We also found a positive significant association between $\delta^{13}C$ and $\delta^{18}O$ only for D trees (ND trees: $F = 0.390$, $p = 0.539$; D trees: $F = 3.537$, $p = 0.049$) (Figure 5b).

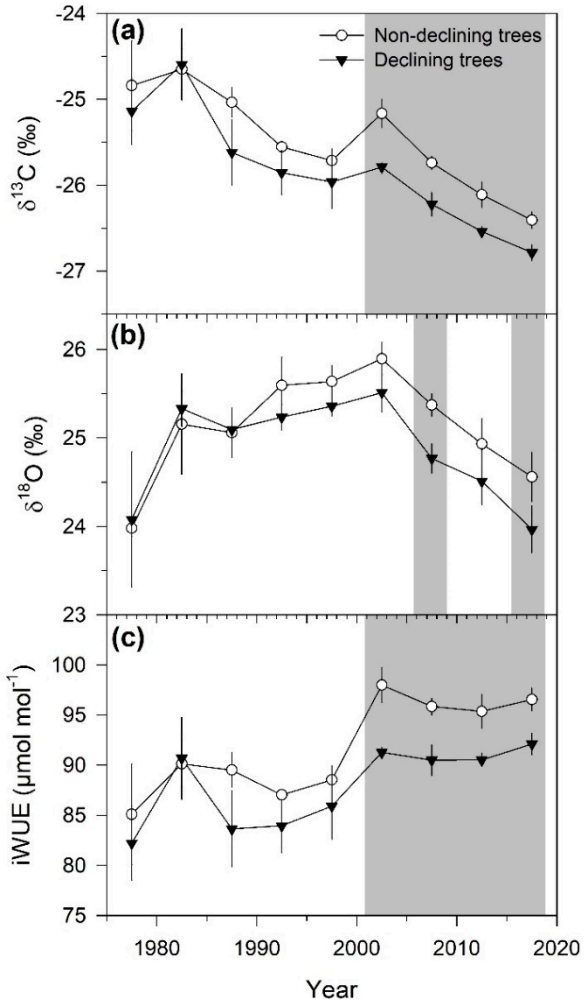

Figure 4. Changes in carbon ($\delta^{13}C$) (**a**) and oxygen ($\delta^{18}O$) (**b**) isotope ratios in tree rings, as well as in intrinsic water-use efficiency (iWUE) (**c**) along the study period in non-declining (empty circles) and declining (black triangles) *Pinus nigra* trees. Symbols represent means ± standard error of each group of five consecutive rings. Significant differences ($p < 0.05$) between tree vigor classes are indicated by grey filled areas.

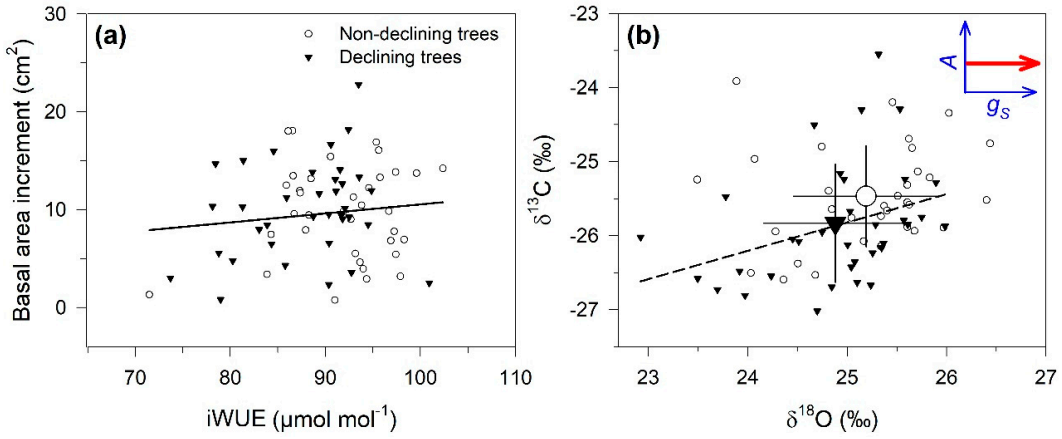

Figure 5. Relationships between basal area increment (BAI) and intrinsic water-use efficiency (iWUE) (**a**) and between carbon ($\delta^{13}C$) and oxygen ($\delta^{18}O$) isotope ratios (**b**) for non-declining (empty circles) and declining (black triangles) *Pinus nigra* trees. Each symbol represents values of five consecutive rings for the entire study period (1975–2018). Big symbols in (**b**) show mean ± standard error values for both tree vigor classes, and the top left inset indicates changes in stomatal conductance (g_S) and photosynthesis (A) according to [32]. Solid and dash lines represent significant associations for ND and D trees, respectively.

4. Discussion

The long-term radial growth patterns of the studied *Pinus nigra* trees were positively associated with water availability at long timescales encompassing the previous autumn to early summer, and the positive effect of water availability on growth was stronger in declining trees than in non-declining trees. Consistently, declining trees exhibited greater impact of severe drought events at both short- and long-term scales, indicated by reduced resilience and negative growth trends, which led to the reduced growth of this vigor class from 2012 onwards. Differences between tree classes could be attributed to the lower stomatal control that declining trees displayed during the last two decades, reflected by lower $\delta^{13}C$ and $\delta^{18}O$ values, which resulted in decreased iWUE in declining trees compared to non-declining ones. Therefore, our results suggest hydraulic failure as the mechanism underlying growth decline and canopy dieback, which could be accentuated by leaf area reduction as a consequence of leaf desiccation.

The negative effect of water shortage on secondary growth, which results in narrow tree rings, is well documented in previous studies [28], and it has strong evidence for southern *P. nigra* populations [21,53,54]. This is also supported by our results (Figure 3). The strongest BAI–SPEI correlations were found at 12-month timescales covering from previous August to current July. Therefore, radial growth relies not only on water balance during spring and early summer, when the radial enlargement of tracheids peaks [16], but also on hydrological conditions recorded during the previous year. Favorable conditions during the previous autumn and winter would not directly influence tree growth, but they would increase soil water reserves for supporting growth during spring [55,56] and enhance carbohydrate accumulation and spring cambial dynamics [57,58] with a positive effect on the growth of earlywood next year [59]. Similar growth responses to long drought timescales (9–15 months) have been reported in studies assessing large water availability gradients in the Iberian Peninsula [55,60], and this pattern has been supported at a global scale [61]. Our study area is located in the transition between the Mediterranean and Atlantic regions, so prevailing conditions are not particularly xeric. However, growth and responses to drought are modulated by site conditions, such as soil type or interaction with neighboring trees [22,62,63]. In fact, strong competition for water resources in xeric sites resulting from high stand density has been proposed to drive higher drought vulnerability in *P. nigra* plantations compared to natural stands [53].

Long-term climate–growth relationships showed a stronger effect of water availability in D trees as compared to ND trees (Figure 3). Consistently, the impact of severe drought events was stronger on

the short- and long-term growth responses of D trees than of ND trees (Table 1). Climate extremes such as droughts have been shown to have a stronger impact on ecological processes than average conditions [64,65]. Indeed, an increase in the global patterns of forest dieback and tree mortality episodes has been primary attributed to droughts and heat waves [1]. Likewise, we argue that the onset of growth decline and dieback symptoms of D trees in our study plantation was triggered by successive severe droughts that would progressively impair physiological processes, in line with previous studies reporting canopy dieback and tree mortality in other natural and planted *P. nigra* forests [6,16,21,53]. The fact that drought resilience was lower in D trees than in ND trees (significant in 2002 and 2012 extreme years), together with the negative growth trends found in D trees after all droughts considered, supports this argument (Table 1). Similarly to other research [66,67], we identified the severe drought in 2012 as a tipping point in the dieback process of D trees, but in this case the drought affected planted stands in a relatively mesic site.

The predisposition to growth decline and canopy dieback in D trees may arise from different water use strategies adopted by the two tree classes. The lower $\delta^{13}C$ and $\delta^{18}O$ in D trees in comparison with the values of ND trees (Figures 4 and 5b), together with the positive association between both isotope signals only found in D trees, indicate a poorer stomatal regulation in declining trees [32]. This water-spending behavior is consistent with the higher growth sensitivity to water supply (Figure 3) and the uncoupling between the growth and iWUE of D trees (Figure 5a). High g_S and associated increased hydraulic efficiency would maximize carbon assimilation and enhance growth under favorable environmental conditions. This prodigal strategy, as defined by Hentschel et al. [36], has previously been reported in *P. nigra* declining populations [21]. However, we did not find differences in growth between the tree vigor classes. Growth is not driven by source activity but by other environmental constraints such as water shortages [68], so seasonal summer drought can shorten the radial enlargement of tracheids, which largely determines final ring width, to a greater extent in D trees [16]. In contrast, lower stomatal control involves a higher risk of xylem cavitation during drought [30]. This is supported by the wider lumen and thinner cell walls of tracheids detected in declining trees of this species [21,69,70] and other gymnosperms [36,71], although the opposite pattern has also been reported for long-term dieback processes (see, for instance, [72]). Savi et al. [70] also found that hydraulic conductivity decreased in declining *P. nigra* trees after the severe drought in 2012, as a possible consequence of embolism accumulated during drought. Furthermore, the impairment of water transport linked to the progressive lower growth rates of D trees can be attributed to cavitation fatigue after successive severe droughts, and this is the phenomenon by which previous cavitation damage enlarges vulnerability to cavitation in following droughts [73].

We are aware that the interpretation of the dual isotope approach presents some caveats, since tree ring $\delta^{18}O$ may also reflect variations in $\delta^{18}O$ in the source water related to changes in soil water uptake depths [34,74]. However, the forest under study is an even-aged reforested stand with homogeneous trees in terms of size or age (no significant differences for DBH and height were found between ND and D trees), thus with comparable root systems. Therefore, we assume that both tree vigor classes took up water from soil sources with similar $\delta^{18}O$ signatures.

Severe droughts can have long-lasting impacts on the leaf area on D trees either as an adaptation mechanism for reducing the transpiring area to compensate for delayed stomatal closure [75], or as a consequence of the reduced efficiency to transport water to foliage and the subsequent leaf desiccation [76,77]. Drought-induced defoliation, together with prolonged periods of near complete stomatal closure, has been related to reductions in non-structural carbohydrate (NSC) concentration in declining pine trees [70,78], thus reducing investment in defensive structures and compounds [26]. Indeed, tree individuals with reduced long-term vigor have been found to be more susceptible to insect outbreaks [29]. At stand level, scattered defoliation by the pine processionary moth detected in the study forest, which particularly affects *P. nigra* [79], could have accentuated the depletion in NSC. Nonetheless, the sampled trees showed neither caterpillar nests or signs of herbivory at the time of sampling, nor growth series exhibiting drops associated to insect attacks (Figure 1a). As a

consequence of defoliation, the photosynthetic area suffered a greater reduction in D trees relative to ND trees, thus impairing carbon assimilation [78] and contributing to the decrease in iWUE and, probably, to a decline in carbon reserves. Although an impending carbon starvation should not be discarded since it has been found to be common among gymnosperms [80], our results only provide evidence for hydraulic failure underlying dieback, which, in fact, is ubiquitous across tree taxa [24].

Finally, we want to pay attention to the similar patterns of growth and carbon and oxygen isotope ratios followed by the two tree vigor classes (Figures 2 and 4). For instance, the $\delta^{13}C$ and $\delta^{18}O$ of ND and D trees were negatively associated before 2000, indicating strong stomatal regulation [32]. However, this relationship became positive after 2000, suggesting a loss in stomatal control in both tree vigor classes, although it was stronger in D trees (see Figure 4a,b). Although ND trees were asymptomatic (showed low defoliation) during the sampling dates, *P. nigra* has been shown to be sensitive to drought considering the thresholds of xylem cavitation [70]. Vulnerability to drought has been reported to be enhanced in forest plantations compared to naturally regenerated forests [13,53]. Furthermore, the subspecies of the study plantation (*P. nigra* subsp. *nigra*) is not native to the Iberian Peninsula, but it is originally from Austria and the Balkan Peninsula (Figure 1a) and typically shows resistance to low temperatures but may be vulnerable to severe drought events. Nevertheless, the differences in physiological traits related to water-use and drought resistance have not been found among European subspecies of *P. nigra* [35].

Pine reforestations in Spain cover ca. $2.6\ 10^6$ ha, of which $3.6\ 10^5$ ha correspond to *P. nigra* plantations [81]. If the frequency and intensity of severe droughts and heat waves increase [8,82], loss of vitality and tree mortality could extent to ND trees of the study plantation and the same fate may follow other plantations of similar characteristics. These dieback and mortality episodes will involve important ecological and economic implications considering the productive and protective role of these planted forests. The systematic implementation of this experimental design (i.e., comparison of co-occurring ND and D trees) including several stands within the species distribution can help to elucidate processes leading to drought-induced dieback [6,75,83]. Studies dealing with drought-vulnerable pine plantations have provided insights into the patterns of growth decline and canopy dieback [13,17]. However, more information is needed for disentangling the underlying physiological mechanisms. The dual-isotope approach offers a unique opportunity in this regard [30,32], as this study proves.

5. Conclusions

Both dendrochronological and stable isotope approaches to tree response to climatic variability provide consistent outcomes and point towards a mechanistic explanation for the dieback of some trees in the studied *P. nigra* plantation. We postulate that reduced stomatal control (low $\delta^{13}C$ and $\delta^{18}O$ signatures) predisposed declining trees to xylem embolism during extreme drought events. The accumulated effect of xylem embolism after successive droughts likely reduced water transport efficiency. Therefore, hydraulic failure is proposed as the physiological mechanism leading to growth decline and canopy dieback. This agrees with the reduced resilience against drought observed in declining trees. In addition, drought-induced leaf area reduction suggests an impairment of photosynthesis, possibly contributing to dieback.

Author Contributions: Conceptualization, E.G.d.A. and J.J.C.; methodology, E.G.d.A. and J.J.C.; software, E.G.d.A. and J.J.C.; validation, E.G.d.A.; formal analysis, E.G.d.A.; data curation, J.J.C.; writing—original draft preparation, E.G.d.A.; writing—review and editing, E.G.d.A. and J.J.C.; funding acquisition, J.J.C. All authors have read and agreed to the published version of the manuscript.

Funding: This research was funded by the Spanish Ministry of Science, Innovation, and Universities, grant number FORMAL (RTI2018-096884-B-C31).

Acknowledgments: We thank several colleagues for their assistance during field and laboratory work, particularly Govt. Navarra Forest Guards. We acknowledge the reviewers and the editor for improving a previous version of the manuscript.

Conflicts of Interest: The authors declare no conflict of interest.

References

1. Allen, C.D.; Macalady, A.K.; Chenchouni, H.; Bachelet, D.; McDowell, N.; Vennetier, M.; Kitzberger, T.; Rigling, A.; Breshears, D.D.; Hogg, E.H.; et al. A global overview of drought and heat-induced tree mortality reveals emerging climate change risks for forests. *For. Ecol. Manage.* **2010**, *259*, 660–684. [CrossRef]
2. Cailleret, M.; Jansen, S.; Robert, E.M.R.; Desoto, L.; Aakala, T.; Antos, J.A.; Beikircher, B.; Bigler, C.; Bugmann, H.; Caccianiga, M.; et al. A synthesis of radial growth patterns preceding tree mortality. *Glob. Chang. Biol.* **2017**, *23*, 1675–1690. [CrossRef]
3. Van Mantgem, P.J.; Stephenson, N.L.; Byrne, J.C.; Daniels, L.D.; Franklin, J.F.; Fulé, P.Z.; Harmon, M.E.; Larson, A.J.; Smith, J.M.; Taylor, A.H.; et al. Widespread increase of tree mortality rates in the Western United States. *Science* **2009**, *323*, 521–524. [PubMed]
4. Peng, C.; Ma, Z.; Lei, X.; Zhu, Q.; Chen, H.; Wang, W.; Liu, S.; Li, W.; Fang, X.; Zhou, X. A drought-induced pervasive increase in tree mortality across Canada's boreal forests. *Nat. Clim. Chang.* **2011**, *1*, 467–471. [CrossRef]
5. Phillips, O.L.; Aragão, L.E.O.C.; Lewis, S.L.; Fisher, J.B.; Lloyd, J.; López-gonzález, G.; Malhi, Y.; Monteagudo, A.; Peacock, J.; Quesada, C.A.; et al. Drought Sensitivity of the Amazon Rainforest. *Science* **2009**, *323*, 1344–1347. [CrossRef] [PubMed]
6. Camarero, J.J.; Gazol, A.; Sangüesa-Barreda, G.; Cantero, A.; Sánchez-Salguero, R.; Sánchez-Miranda, A.; Granda, E.; Serra-Maluquer, X.; Ibáñez, R. Forest growth responses to drought at short- and long-term scales in Spain: Squeezing the stress memory from tree rings. *Front. Ecol. Evol.* **2018**, *6*, 1–11. [CrossRef]
7. Steinkamp, J.; Hickler, T. Is drought-induced forest dieback globally increasing? *J. Ecol.* **2015**, *103*, 31–43. [CrossRef]
8. Christidis, N.; Jones, G.S.; Stott, P.A. Dramatically increasing chance of extremely hot summers since the 2003 European heatwave. *Nat. Clim. Chang.* **2015**, *5*, 46–50. [CrossRef]
9. Zhou, S.; Zhang, Y.; Williams, A.P.; Gentine, P. Projected increases in intensity, frequency, and terrestrial carbon costs of compound drought and aridity events. *Sci. Adv.* **2019**, *5*, 1–9. [CrossRef] [PubMed]
10. Allen, C.D.; Breshears, D.D.; McDowell, N.G. On underestimation of global vulnerability to tree mortality and forest die-off from hotter drought in the Anthropocene. *Ecosphere* **2015**, *6*, 1–55. [CrossRef]
11. Anderegg, W.R.L.; Kane, J.M.; Anderegg, L.D.L. Consequences of widespread tree mortality triggered by drought and temperature stress. *Nat. Clim. Chang.* **2013**, *3*, 30–36. [CrossRef]
12. Song, L.; Li, M.; Zhu, J.; Zhang, J. Comparisons of radial growth and tree-ring cellulose δ13C for *Pinus sylvestris* var. *mongolica* in natural and plantation forests on sandy lands. *J. For. Res.* **2017**, *22*, 160–168.
13. Navarro-Cerrillo, R.M.; Rodriguez-Vallejo, C.; Silveiro, E.; Hortal, A.; Palacios-Rodríguez, G.; Duque-Lazo, J.; Camarero, J.J. Cumulative drought stress leads to a loss of growth resilience and explains higher mortality in planted than in naturally regenerated Pinus pinaster stands. *Forests* **2018**, *9*, 358. [CrossRef]
14. FAO. *Global Forest Resources Assessment*; FAO: Rome, Italy, 2010.
15. Sánchez-Salguero, R.; Navarro-Cerrillo, R.M.; Camarero, J.J.; Fernández-Cancio, Á. Selective drought-induced decline of pine species in southeastern Spain. *Clim. Change* **2012**, *113*, 767–785. [CrossRef]
16. Guada, G.; Camarero, J.J.; Sánchez-Salguero, R.; Cerrillo, R.M.N. Limited growth recovery after drought-induced forest dieback in very defoliated trees of two pine species. *Front. Plant Sci.* **2016**, *7*, 1–12. [CrossRef]
17. Sánchez-Salguero, R.; Navarro-Cerrillo, R.M.; Swetnam, T.W.; Zavala, M.A. Is drought the main decline factor at the rear edge of Europe? The case of southern Iberian pine plantations. *For. Ecol. Manage.* **2012**, *271*, 158–169. [CrossRef]
18. Sangüesa-Barreda, G.; Linares, J.C.; Camarero, J.J. Reduced growth sensitivity to climate in bark-beetle infested Aleppo pines: Connecting climatic and biotic drivers of forest dieback. *For. Ecol. Manage.* **2015**, *357*, 126–137. [CrossRef]
19. Dorman, M.; Perevolotsky, A.; Sarris, D.; Svoray, T. The effect of rainfall and competition intensity on forest response to drought: Lessons learned from a dry extreme. *Oecologia* **2015**, *177*, 1025–1038. [CrossRef]
20. García de la Serrana, R.; Vilagrosa, A.; Alloza, J.A. Pine mortality in southeast Spain after an extreme dry and warm year: Interactions among drought stress, carbohydrates and bark beetle attack. *Trees Struct. Funct.* **2015**, *29*, 1791–1804. [CrossRef]

21. Petrucco, L.; Nardini, A.; Von Arx, G.; Saurer, M.; Cherubini, P. Isotope signals and anatomical features in tree rings suggest a role for hydraulic strategies in diffuse drought-induced die-back of Pinus nigra. *Tree Physiol.* **2017**, *37*, 523–535.
22. McDowell, N.; Pockman, W.T.; Allen, C.D.; Breshears, D.D.; Cobb, N.; Kolb, T.; Plaut, J.; Sperry, J.; West, A.; Williams, D.G.; et al. Mechanisms of plant survival and mortality during drought: Why do some plants survive while others succumb to drought? *New Phytol.* **2008**, *178*, 719–739. [CrossRef]
23. Anderegg, W.R.L.; Berry, J.A.; Smith, D.D.; Sperry, J.S.; Anderegg, L.D.L.; Field, C.B. The roles of hydraulic and carbon stress in a widespread climate-induced forest die-off. *Proc. Natl. Acad. Sci. USA* **2012**, *109*, 233–237. [CrossRef]
24. Adams, H.D.; Zeppel, M.J.B.; Anderegg, W.R.L.; Hartmann, H.; Landhäusser, S.M.; Tissue, D.T.; Huxman, T.E.; Hudson, P.J.; Franz, T.E.; Allen, C.D.; et al. A multi-species synthesis of physiological mechanisms in drought-induced tree mortality. *Nat. Ecol. Evol.* **2017**, *1*, 1285–1291. [CrossRef]
25. McDowell, N.G.; Beerling, D.J.; Breshears, D.D.; Fisher, R.A.; Raffa, K.F.; Stitt, M. The interdependence of mechanisms underlying climate-driven vegetation mortality. *Trends Ecol. Evol.* **2011**, *26*, 523–532. [CrossRef]
26. Anderegg, W.R.L.; Hicke, J.A.; Fisher, R.A.; Allen, C.D.; Aukema, J.; Bentz, B.; Hood, S.; Lichstein, J.W.; Macalady, A.K.; Mcdowell, N.; et al. Tree mortality from drought, insects, and their interactions in a changing climate. *N. Phytol.* **2015**, *208*, 674–683. [CrossRef]
27. Gessler, A.; Schaub, M.; McDowell, N.G. The role of nutrients in drought-induced tree mortality and recovery. *N. Phytol.* **2017**, *214*, 513–520. [CrossRef]
28. Fritts, H.C. *Tree Rings and Climate*; Academic Press: London, UK, 2001.
29. Knapp, P.A.; Soulé, P.T.; Maxwell, J.T. Mountain pine beetle selectivity in old-growth ponderosa pine forests, Montana, USA. *Ecol. Evol.* **2013**, *3*, 1141–1148. [CrossRef]
30. Gessler, A.; Cailleret, M.; Joseph, J.; Schönbeck, L.; Schaub, M.; Lehmann, M.; Treydte, K.; Rigling, A.; Timofeeva, G.; Saurer, M. Drought induced tree mortality—A tree-ring isotope based conceptual model to assess mechanisms and predispositions. *N. Phytol.* **2018**, *219*, 485–490. [CrossRef]
31. Farquhar, G.D.; O'Leary, M.H.; Berry, J.A. On the relationship between carbon isotope discrimination and the intercellular carbon dioxide concentration in leaves. *Aust. J. Plant Physiol.* **1982**, *9*, 121–137. [CrossRef]
32. Scheidegger, Y.; Saurer, M.; Bahn, M.; Siegwolf, R. Linking stable oxygen and carbon isotopes with stomatal conductance and photosynthetic capacity: A conceptual model. *Oecologia* **2000**, *125*, 350–357. [CrossRef]
33. Gessler, A.; Löw, M.; Heerdt, C.; Beeck, M.O.D.; Schumacher, J.; Grams, T.E.E.; Bahnweg, G.; Ceulemans, R.; Werner, H.; Matyssek, R.; et al. Within-canopy and ozone fumigation effects on δ13C and Δ18O in adult beech (Fagus sylvatica) trees: Relation to meteorological and gas exchange parameters. *Tree Physiol.* **2009**, *29*, 1349–1365. [CrossRef]
34. Roden, J.; Siegwolf, R. Is the dual-isotope conceptual model fully operational? *Tree Physiol.* **2012**, *32*, 1179–1182. [CrossRef]
35. Santini, F.; Serrano, L.; Kefauver, S.C.; Abdullah-Al, M.; Aguilera, M.; Sin, E.; Voltas, J. Morpho-physiological variability of Pinus nigra populations reveals climate-driven local adaptation but weak water use differentiation. *Environ. Exp. Bot.* **2019**, *166*, 103828. [CrossRef]
36. Hentschel, R.; Rosner, S.; Kayler, Z.E.; Andreassen, K.; Børja, I.; Solberg, S.; Einar, O.; Priesack, E.; Gessler, A. Norway spruce physiological and anatomical predisposition to dieback. *For. Ecol. Manage.* **2014**, *322*, 27–36. [CrossRef]
37. Caudullo, G.; Welk, E.; San-miguel-ayanz, J. Chorological maps for the main European woody species. *Data Br.* **2017**, *12*, 662–666. [CrossRef]
38. Droogers, P.; Allen, R.G. Estimating reference evapotranspiration under inaccurate data conditions. *Irrig. Drain. Syst.* **2002**, *16*, 33–45. [CrossRef]
39. Vicente-Serrano, S.M.; Beguería, S.; López-Moreno, J.I. A multiscalar drought index sensitive to global warming: The standardized precipitation evapotranspiration index. *J. Clim.* **2010**, *23*, 1696–1718. [CrossRef]
40. Holmes, R.L. Computer-Assisted Quality Control in Tree-Ring Dating and Measurement. *Tree-Ring Bull.* **1983**, *43*, 69–78.
41. Biondi, F.; Qeadan, F. A Theory-Driven Approach to Tree-Ring Standardization: Defining the Biological Trend from Expected Basal Area Increment. *Tree-Ring Res.* **2008**, *64*, 81–96. [CrossRef]

42. Lloret, F.; Keeling, E.G.; Sala, A. Components of tree resilience: Effects of successive low-growth episodes in old ponderosa pine forests. *Oikos* **2011**, *120*, 1909–1920. [CrossRef]
43. Gazol, A.; Ribas, M.; Gutiérrez, E.; Camarero, J.J. Aleppo pine forests from across Spain show drought-induced growth decline and partial recovery. *Agric. For. Meteorol.* **2017**, *232*, 186–194. [CrossRef]
44. Boettger, T.; Haupt, M.; Knöller, K.; Weise, S.M.; Waterhouse, J.S.; Rinne, K.T.; Loader, N.J.; Sonninen, E.; Jungner, H.; Masson-Delmotte, V.; et al. Wood cellulose preparation methods and mass spectrometric analyses of δ13C, δ18O, and nonexchangeable δ2H values in cellulose, sugar, and starch: An interlaboratory comparison. *Anal. Chem.* **2007**, *79*, 4603–4612. [CrossRef] [PubMed]
45. Sharp, Z. *Principles of Stable Isotope Geochemistry*. 2005. Available online: https://www.amazon.com/Principles-Stable-Isotope-Geochemistry-Zachary/dp/0130091391 (accessed on 2 November 2020).
46. McCarroll, D.; Loader, N.J. Stable isotopes in tree rings. *Quat. Sci. Rev.* **2004**, *23*, 771–801. [CrossRef]
47. Pinheiro, J.C.; Bates, D.M. *Mixed-Effects Models in S and S-PLUS.*; Springer: New York, NY, USA, 2000.
48. *R Core Team R: A Language and Environment for Statistical Computing*; R Foundation for Statistical Computing: Vienna, Austria, 2020.
49. Beguería, S.; Vicente-Serrano, S.M. *SPEI: Calculation of the Standardised Precipitation-Evapotranspiration Index*; R package Version 1.7. 2017. Available online: https://CRAN.R-project.org/package=SPEI (accessed on 8 December 2017).
50. Bunn, A.; Korpela, M.; Biondi, F.; Campelo, F.; Mérian, P.; Qeadan, F.; Zang, C. *dplR: Dendrochronology Program Library in R.*; R Package Version 1.7.1. 2020. Available online: https://CRAN.R-project.org/package=dplR (accessed on 10 December 2020).
51. McLeod, A.I. *Kendall: Kendall Rank Correlation and Mann-Kendall Trend Test*; R Package Version 2.2. 2011. Available online: https://CRAN.R-project.org/package=Kendall (accessed on 25 August 2011).
52. Pinheiro, J.; Bates, D.; DebRoy, S.; Sarkar, D.; Team, R.C. *Nlme: Linear and Nonlinear Mixed Effects Models*; R Package Version 3.1-145. 2020. Available online: https://CRAN.R-project.org/package=nlme (accessed on 10 December 2020).
53. Sánchez-Salguero, R.; Camarero, J.J.; Dobbertin, M.; Fernández-Cancio, T.; Vilà-Cabrera, A.; Manzanedo, R.D.; Zavala, M.A.; Navarro-Cerrillo, R.M. Contrasting vulnerability and resilience to drought-induced decline of densely planted vs. natural rear-edge Pinus nigra forests. *For. Ecol. Manage.* **2013**, *310*, 956–967. [CrossRef]
54. Linares, J.C.; Tíscar, P.A. Climate change impacts and vulnerability of the southern populations of Pinus nigra subsp. salzmannii. *Tree Physiol.* **2010**, *30*, 795–806. [CrossRef]
55. Pasho, E.; Camarero, J.J.; de Luis, M.; Vicente-Serrano, S.M. Impacts of drought at different time scales on forest growth across a wide climatic gradient in north-eastern Spain. *Agric. For. Meteorol.* **2011**, *151*, 1800–1811. [CrossRef]
56. Sarris, D.; Christodoulakis, D.; Körner, C. Recent decline in precipitation and tree growth in the eastern Mediterranean. *Glob. Chang. Biol.* **2007**, *13*, 1187–1200. [CrossRef]
57. Vaganov, E.A.; Hughes, M.K.; Shaskin, A.V. *Growth Dynamics of Conifer Tree Rings-Images of Past and Futures Environments*; Springer: Berlin/Heidelberg, Germany, 2006.
58. Hoch, G.; Richter, A.; Körner, C. Non-structural carbon compounds in temperate forest trees. *Plant Cell Environ.* **2003**, *26*, 1067–1081. [CrossRef]
59. Martín-Benito, D.; Cherubini, P.; del Río, M.; Cañellas, I. Growth response to climate and drought in Pinus nigra Arn. trees of different crown classes. *Trees* **2008**, *22*, 363–373. [CrossRef]
60. Gazol, A.; Camarero, J.J.; Sánchez-Salguero, R.; Vicente-Serrano, S.M.; Serra-Maluquer, X.; Gutiérrez, E.; de Luis, M.; Sangüesa-Barreda, G.; Novak, K.; Rozas, V.; et al. Drought legacies are short, prevail in dry conifer forests and depend on growth variability. *J. Ecol.* **2020**, *108*, 2473–2484. [CrossRef]
61. Vicente-Serrano, S.M.; Camarero, J.J.; Azorin-Molina, C. Diverse responses of forest growth to drought time-scales in the Northern Hemisphere. *Glob. Ecol. Biogeogr.* **2014**, *23*, 1019–1030. [CrossRef]
62. Linares, J.C.; Camarero, J.J.; Carreira, J.A. Competition modulates the adaptation capacity of forests to climatic stress: Insights from recent growth decline and death in relict stands of the Mediterranean fir Abies pinsapo. *J. Ecol.* **2010**, *98*, 592–603. [CrossRef]
63. González de Andrés, E.; Camarero, J.J.; Blanco, J.A.; Imbert, J.B.; Lo, Y.H.; Sangüesa-Barreda, G.; Castillo, F.J. Tree-to-tree competition in mixed European beech–Scots pine forests has different impacts on growth and water-use efficiency depending on site conditions. *J. Ecol.* **2018**, *106*, 59–75. [CrossRef]

64. Medvigy, D.; Wofsy, S.C.; Munger, J.W.; Moorcroft, P.R. Responses of terrestrial ecosystems and carbon budgets to current and future environmental variability. *Proc. Natl. Acad. Sci. USA* **2010**, *107*, 8275–8280. [CrossRef] [PubMed]
65. Smith, M.D. The ecological role of climate extremes: Current understanding and future prospects. *J. Ecol.* **2011**, *99*, 651–655. [CrossRef]
66. Camarero, J.J.; Gazol, A.; Sangüesa-Barreda, G.; Oliva, J.; Vicente-Serrano, S.M. To die or not to die: Early warnings of tree dieback in response to a severe drought. *J. Ecol.* **2015**, *103*, 44–57. [CrossRef]
67. Chaparro, D.; Vayreda, J.; Vall-Ilossera, M.; Banqué, M.; Piles, M.; Camps, A.; Martínez-Vilalta, J. The role of climatic anomalies and soil moisture in the decline of drought-prone forests. *IEEE J. Sel. Top. Appl. Earth Obs. Remote Sens.* **2017**, *10*, 503–514. [CrossRef]
68. Körner, C. Paradigm shift in plant growth control. *Curr. Opin. Plant Biol.* **2015**, *25*, 107–114. [CrossRef]
69. Martin-Benito, D.; Beeckman, H.; Cañellas, I. Influence of drought on tree rings and tracheid features of Pinus nigra and Pinus sylvestris in a mesic Mediterranean forest. *Eur. J. For. Res.* **2013**, *132*, 33–45. [CrossRef]
70. Savi, T.; Casolo, V.; Dal Borgo, A.; Rosner, S.; Torboli, V.; Stenni, B.; Bertoncin, P.; Martellos, S.; Pallavicini, A.; Nardini, A. Drought-induced dieback of Pinus nigra: A tale of hydraulic failure and carbon starvation. *Conserv. Physiol.* **2019**, *7*, 1–12.
71. Voltas, J.; Camarero, J.J.; Carulla, D.; Aguilera, M.; Ortiz, A.; Ferrio, J.P. A retrospective, dual-isotope approach reveals individual predispositions to winter-drought induced tree dieback in the southernmost distribution limit of Scots pine. *Plant Cell Environ.* **2013**, 1435–1448. [CrossRef]
72. Pellizzari, E.; Camarero, J.J.; Gazol, A.; Sangüesa-Barreda, G.; Carrer, M. Wood anatomy and carbon-isotope discrimination support long-term hydraulic deterioration as a major cause of drought-induced dieback. *Glob. Chang. Biol.* **2016**, *22*, 2125–2137. [CrossRef]
73. Hacke, U.G.; Stiller, V.; Sperry, J.S.; Pittermann, J.; Mcculloh, K.A. Cavitation Fatigue. Embolism and Refilling Cycles Can Weaken the Cavitation Resistance of Xylem 1. *Plant Physiol.* **2001**. [CrossRef] [PubMed]
74. Gessler, A.; Ferrio, J.P.; Hommel, R.; Treydte, K.; Werner, R.A.; Monson, R.K. Stable isotopes in tree rings: Towards a mechanistic understanding of isotope fractionation and mixing processes from the leaves to the wood. *Tree Physiol.* **2014**, *34*, 796–818. [CrossRef] [PubMed]
75. Colangelo, M.; Camarero, J.J.; Battipaglia, G.; Borghetti, M.; De Micco, V.; Gentilesca, T.; Ripullone, F. A multi-proxy assessment of dieback causes in a Mediterranean oak species. *Tree Physiol.* **2017**, *37*, 617–631. [CrossRef] [PubMed]
76. Bréda, N.; Roland, H.; Granier, A.; Dreyer, E. Temperate forest trees and stands under severe drought: A review of ecophysiological responses, adaptation processes and long-term consequences. *Ann. For. Sci.* **2006**, *63*, 625–644. [CrossRef]
77. Jump, A.S.; Ruiz-Benito, P.; Greenwood, S.; Allen, C.D.; Kitzberger, T.; Fensham, R.; Martínez-Vilalta, J.; Lloret, F. Structural overshoot of tree growth with climate variability and the global spectrum of drought-induced forest dieback. *Glob. Chang. Biol.* **2017**, *23*, 3742–3757. [CrossRef]
78. Poyatos, R.; Aguadé, D.; Galiano, L.; Mencuccini, M.; Martínez-Vilalta, J. Drought-induced defoliation and long periods of near-zero gas exchange play a key role in accentuating metabolic decline of Scots pine. *N. Phytol.* **2013**, *200*, 388–401. [CrossRef]
79. Gazol, A.; Hernández-Alonso, R.; Camarero, J.J. Patterns and Drivers of Pine Processionary Moth Defoliation in Mediterranean Mountain Forests. *Front. Ecol. Evol.* **2019**, *7*, 1–9. [CrossRef]
80. Martínez-Vilalta, J.; Sala, A.; Asensio, D.; Galiano, L.; Hoch, G.; Palacio, S.; Piper, F.I.; Lloret, F. Dynamics of non-structural carbohydrates in terrestrial plants: A global synthesis. *Ecol. Monogr.* **2016**, *86*, 495–516. [CrossRef]
81. Vadell Guiral, E.; de Miguel Magaña, S.; Pemán García, J. La actividad repobladora desarrollada a partir de 1940. Luces y sombras. In *La restauración Forestal de España: 75 Años de Una Ilusión*; Pemán García, J., Iriarte Goñi, I., Lario Leza, F.J., Eds.; Ministerio de Agricultura y Pesca, Alimentación y Medio Ambiente, Gobierno de España: Madrid, Spain, 2017; pp. 175–226.
82. Coll, J.R.; Jones, P.D.; Aguilar, E. Expected changes in mean seasonal precipitation and temperature across the Iberian Peninsula for the 21st century. *Idojaras* **2015**, *119*, 1–21.

83. Sánchez-Salguero, R.; Colangelo, M.; Matías, L.; Ripullone, F.; Camarero, J.J. Shifts in growth responses to climate and exceeded drought-vulnerability thresholds characterize dieback in two Mediterranean deciduous oaks. *Forests* **2020**, *11*, 714. [CrossRef]